Journal of Alloys and Compounds 605 (2014) 12–20

Contents lists available at ScienceDirect

Journal of Alloys and Compounds

journal homepage: www.elsevier.com/locate/jalcom

Cold metal transfer welding–brazing of pure titanium TA2 to magnesium alloy AZ31B

R. Cao *, T. Wang, C. Wang, Z. Feng, Q. Lin, J.H. Chen

State Key Laboratory of Advanced Processing and Recycling of Non-ferrous Metals, Lanzhou University of Technology, Lanzhou 730050, PR China
Key Laboratory of Non-ferrous Metal Alloys of Ministry of Education, Lanzhou University of Technology, Lanzhou 730050, PR China

ARTICLE INFO

Article history:
Received 16 November 2013
Received in revised form 8 March 2014
Accepted 10 March 2014
Available online 26 March 2014

Keywords:
Ti/Mg dissimilar alloys
CMT welding–brazing
Intermetallic compounds (IMCs)
Mechanical property

ABSTRACT

Pure titanium TA2 was joined to Mg AZ31B by cold metal transfer (CMT) welding–brazing method in the form of two lap-shear joints (Mg–Ti joint and Ti–Mg joint) with Mg AZ61 wire. The microstructure of Ti/Mg CMT joints was identified and characterized by means of optical microscopy (OM), scanning electron microscope (SEM), energy dispersive spectroscopy (EDS) and X-ray diffraction (XRD). The mechanical properties of various welding parameters were compared and analyzed. Desired Ti/Mg CMT joints with satisfied weld appearances and mechanical properties were achieved at suitable welding variables. The Ti/Mg CMT joints had dual characteristics of a welding joint at the Mg side and a brazing joint at the Ti side. Moreover, for two joints, the brazing interfaces were composed of an intermetallic compounds (IMCs) layer including Ti_3Al, $Mg_{17}Al_{12}$ and $Mg_{0.97}Zn_{0.03}$ phases. Mg–Ti joint had the higher tensile load of 2.10 kN, and Ti–Mg joint had the tensile load of 1.83 kN.

1. Introduction

In modern engineering industries, the use of welded structures of dissimilar alloys can not only make full use of the properties of the materials, but also save rare metals and reduce the cost of the entire structure, such as joining of Ti–Al [1–4], Cu–Al [5–7], Al-steel [8–13], Ti–Cu [14–16], Mg-steel [17–20]. The hybrid structure of Mg–Ti dissimilar alloys is an attractive design in this field [21–26]. However, the welding of magnesium and titanium alloys is very difficult because of the great differences between physical and chemical properties of these two metals. Furthermore, fusion joining of Mg alloy to Ti alloy has a metallurgical challenge due to lower mutual-solubility and lack of reaction [27].

Currently, various methods such as laser welding, friction welding, and liquid diffusion welding methods have been used to join Mg alloys and Ti alloys. Process parameters, properties, and bonding mechanism by laser keyhole welding dissimilar Ti–6Al–4 V titanium alloy to AZ31B magnesium alloy were investigated [22]. Results found that offset from the laser beam center on AZ31B side to the edge of the weld seam played an important role in the properties of the joint. When the optimal range of the offset was from 0.3 mm to 0.4 mm, the joint reached the maximum ultimate tensile strength of 266 MPa. The properties of the joints were related to the composites of the brazing interface. The interfacial layer of acceptable joint was composed of α-Mg and Mg–Al eutectic, while that of bad joint mainly consisted of α-Mg, which attaches on the solid Ti surface directly [23].

Mg alloys and Ti alloys were also joined with middle Al interlayer by transient liquid phase (TLP) method [24]. Results indicated that Al interlayer played a key effect on joining of Mg alloys and Ti alloys. The shear strength of the joint after bonding at 470 °C for 180 min reached 72.4 MPa which was 84.2% of that of AZ31B base metal (86.0 MPa). And the joints were joined by $Mg_{17}Al_{12}$ and Ti_3Al phases in the bonding interface.

A solid-state welding technique, FSW, was also introduced to join commercially titanium and magnesium alloy. The friction heat generation and atom diffusion behavior during Mg–Ti friction welding process were studied, and the results show that the friction coefficient mainly experiences two steady stages. The first steady stage corresponds to the coulomb friction with material abrasion. The second steady stage corresponds to the stick friction with fully plastic flow. It can also be found that the rapid diffusion phenomenon exists in the Mg–Ti friction welding system. The large deformation activated diffusion coefficient is about 10^5 higher than that activated by thermal [25]. Study found Zn and Zr of alloying elements of Mg–Zn–Zr alloy also improved the tensile strength of titanium and magnesium joints by forming the thin reaction layer at the joint interface during friction stir welding

* Corresponding author at: State Key Laboratory of Advanced Processing and Recycling of Non-ferrous Metals, Lanzhou University of Technology, Lanzhou 730050, PR China. Tel.: +86 931 2973529; fax: +86 931 2976578.
E-mail address: caorui@lut.cn (R. Cao).

http://dx.doi.org/10.1016/j.jallcom.2014.03.051
0925-8388/

[26]. Results also indicated that Mg–Al–Zn alloy and Ti butt joints were joined by Al-rich thin layers and Ti–Al intermetallic compound layers formed at the interface of these joints. The thickness of the intermetallic compound layer increased with increasing aluminum content of the Mg–Al–Zn alloy.

As we known, titanium and magnesium do not form a solid solution and any compounds [27]. This means that it is difficult to directly join pure titanium and pure magnesium. Above series results found that the content of aluminum of the magnesium alloy affected the interfacial microstructure and the tensile strength of the dissimilar joint. Therefore, to join Mg AZ31 and pure titanium, a wire including element Al should be chosen.

Recently, cold metal transfer (CMT) joining technique was introduced as a new way to join dissimilar metals [28], especially for the dissimilar metals with a greater difference in melting points [4,11–14,16,17]. The melting points of Mg and Ti are 649 °C and 1668 °C, respectively. This huge difference in melting points makes it very difficult to melt both in one welding pool. In this study, a welding–brazing process by CMT joining technology was carried out to join pure titanium TA2 and Mg AZ31B.

The objective of the current work was to achieve the effective joints of Ti/Mg dissimilar metals by CMT welding–brazing method. The influences of different lapping configuration on the weld appearance and the stability of the welding process were investigated. For the lapping joints with titanium sheet on the top of magnesium sheet or the lapping joints with magnesium sheet on the top of titanium sheet, the macroscopic and microscopic characteristics of the welding–brazing joints as well as the bonding mechanisms of the joints were analyzed. Finally, the tensile strength of the joints with various welding parameters was discussed.

2. Experimental procedures

2.1. Materials

The materials used in this study included 1 mm thick Mg AZ31B alloy sheet and 1 mm thick pure Ti TA2 sheet. The Mg AZ61 wire with a diameter of 1.2 mm was used. Table 1 provided the nominal chemical compositions of TA2 sheet, AZ31B sheet and AZ61 wire.

The two sheets were degreased by acetone and polished by abrasive cloth first. Then magnesium sheets were wiped and rinsed with ethanol. The titanium sheets were cleaned with 20%HNO_3 + 5%HF acid solution for 5 min, then wiped and rinsed with ethanol and tap water.

2.2. Experimental details

The Ti TA2 and the Mg AZ31B sheets used in the lap-shear joint configuration, shown in Fig. 1, were machined to rectangular strips of 200 mm × 50 mm. As shown in Fig. 1, two different configurations of Mg AZ31B to Ti TA2 lap-shear joints were adopted in the experiments with an overlap distance of 10 mm. The Mg–Ti joint presented that the Mg AZ31 sheet was placed on the top of the Ti TA2 sheet as shown in Fig. 1(a), and the Ti–Mg joint presented that the Ti TA2 sheet was placed on the top of the Mg AZ31 sheet as shown in Fig. 1(b). The angle between the welding torch and the normal to the lap seam was 45° away from the direction of welding. The welding direction was parallel to the lapped seam. The deviated distance (D) was defined as the deviation from the wire to the edge of the lapped weld seam. To examine the quality of CMT welding–brazing joint, the cross sections of the specimens were cut from the weldment perpendicular to the welding direction. The ground and polished magnesium and titanium workpieces were etched by using the mixed solution (5 g picric acid +10 ml distilled water +50 ml ethanol +5 g acetic acid) for 30 s at room temperature. The microstructures of the welded joints were observed by optical microscope (OM) and scanning electron microscope (SEM JSM-6700F) equipped with energy dispersive X-ray spectrometer (EDS).

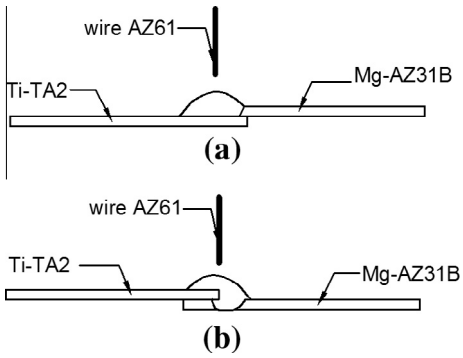

Fig. 1. Schematic of CMT welding of Mg AZ31–titanium TA2 sheet: (a) Mg–Ti joint (top Mg sheet–bottom Ti sheet), and (b) Ti–Mg joint (top Ti sheet–bottom Mg sheet) (dimensions in mm).

In order to investigate the mechanical properties of the CMT welded specimens, static tensile tests were carried out. Specimens in Fig. 2 machined from the weldment were subjected to quasi-static tensile loading on a CSS-2205 testing machine. To minimize the inherent bending stresses during tensile processes of lap shear specimens, filler plates were attached to both ends of the sample using masking tape to accommodate the sample offset. Load vs. displacement curves were obtained at a stroke rate of 1 mm/min. The joint strength was evaluated by the peak load. Two to three replicates were performed, and the average peak loads were reported.

3. Results and discussion

3.1. Effects of welding variables on weld appearance of Mg–Ti joint

3.1.1. Effects of wire feed speed on weld appearance of Mg–Ti joint

To obtain satisfied weld appearance of Mg–Ti joint shown in Fig. 1(a), the effects of various welding variables on weld appearance of Mg–Ti joint were investigated. Fig. 3 showed the effects of wire feed speed on the weld appearance of Mg–Ti joint. In these tests, constant welding speed of 7.14 mm/s was chosen. As shown in Fig. 3(a–c), when the wire feed speed was in the range of 3.5–4.5 m/min, uniform welds were formed. Because at the slowest wire feed speed, the insufficient weld metals made the weld undercut. On the other hand, the smaller heat input induced by the slower wire feed speed led smaller Ti sheet molten. With increasing of the wire feed speed, the increased molten weld metals made the weld appearance become well. As wire feed speed was 5.0 m/min, continuous, smooth and uniform weld appearance without undercutting was produced. However, when the wire feed speed was further increasing, the welding process became unstable, and more spatters and undercutting appeared. Moreover, faster wire feed speed was also disturbing the welding voltage, which induced the disturbance of arc regulation and the unstable welding processes, and thus the discontinuous weld metal was formed.

3.1.2. Effects of welding voltage on weld appearance of Mg–Ti joint

Fig. 4 presents the weld appearance with different welding voltages for Mg–Ti joint. From Fig. 4, with increasing welding voltage, the width of the weld became larger. When the welding voltage of 13 V, wire feed speed of 5.0 m/min and welding speed of 7.14 mm/

Table 1
Nominal chemical composition of Mg AZ31B sheet, Ti TA2 sheet, and Mg AZ61 wire (wt.%).

Alloys	C	H	O	N	Al	Zn	Mn	Ca	Si	Cu	Ni	Ti	Fe	Mg
AZ31B	–	–	–	–	2.9	0.9	0.35	0.04	0.10	0.05	0.005	–	0.005	Bal.
TA2	0.10	0.015	0.25	0.05	–	–	–	–	–	–	–	Bal.	0.30	–
AZ61	–	–	–	–	6.5	0.9	0.15	–	0.30	0.05	0.005	–	0.005	Bal.

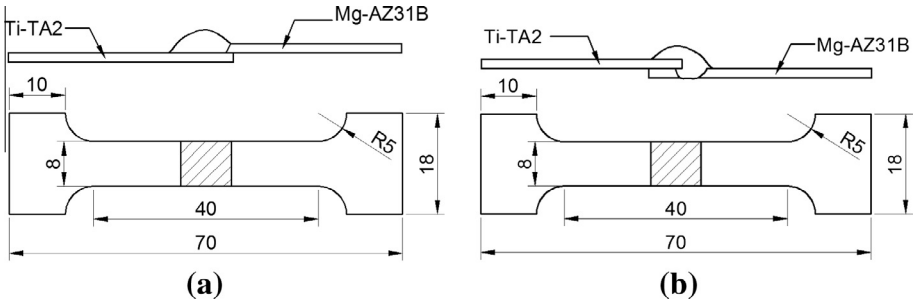

Fig. 2. Specimens machined from the welded Mg AZ31–TA2 sheets: (a) Mg–Ti joint (top Mg sheet–bottom Ti sheet), and (b) Ti–Mg joint (top Ti sheet–bottom Mg sheet) (dimensions in mm).

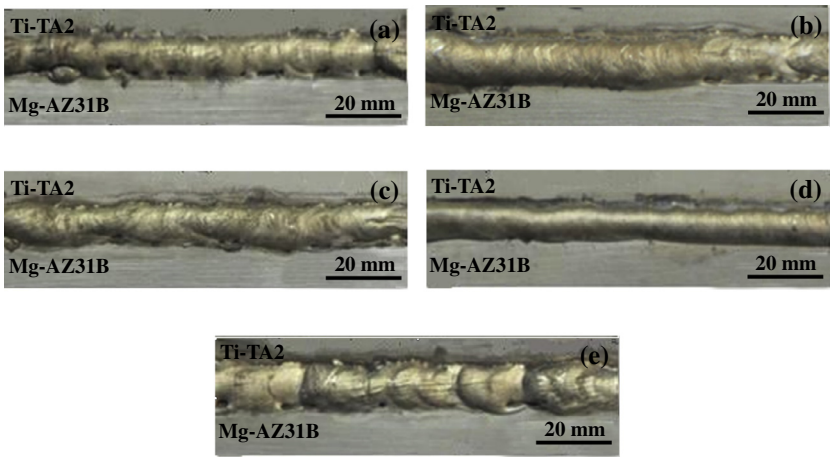

Fig. 3. Effects of wire feed speed on weld appearance for Mg–Ti joint (top Mg sheet–bottom Ti sheet): (a) wire feed speed of 3.5 m/min, (b) wire feed speed of 4.0 m/min, (c) wire feed speed of 4.5 m/min, (d) wire feed speed of 5.0 m/min, and (e) wire feed speed of 6.0 m/min.

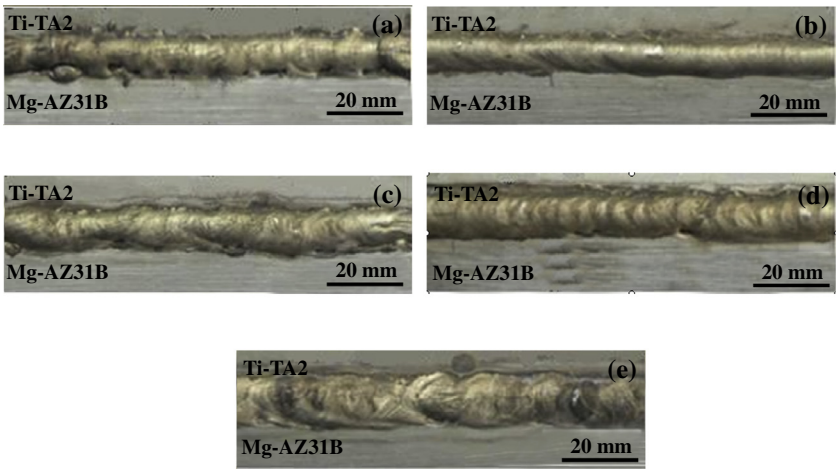

Fig. 4. Effects of welding voltage on weld appearance for Mg–Ti joint (top Mg sheet–bottom Ti sheet): (a) welding voltage of 10 V, (b) welding voltage of 13 V, (c) welding voltage of 15 V, (d) welding voltage of 17 V, and (e) welding voltage of 19 V.

s were chosen, the uniform, continuous weld appearance was formed. Lower welding voltage made molten Mg base metal insufficient. However, higher welding voltage made the width of the weld larger, which led weld metal insufficiently spread on the Ti base metal. Moreover, larger welding voltage induced welding processes unstable, more spatter and infusion defects.

Combined the above series of tests, to obtain satisfied weld appearance of the Mg–Ti joint, the optimized welding variables were obtained at welding voltage of 13 V, wire feed speed of 4.0–5.0 m/min and welding speed of 7.14 mm/s.

3.1.3. Effects of welding voltage on weld appearance of Ti–Mg joint

For Ti–Mg joint as shown in Fig. 1(b), wire feed speed of 5.0 m/min, welding speed of 7.14 mm/s were used, only welding voltage was changed to study the effects of welding voltage on weld

appearance of Ti–Mg joint. Corresponded weld appearances were shown in Fig. 5.

The effects of welding voltage on weld appearance of Ti–Mg joint were similar to Fig. 4. When the welding voltage was in the range of 10–11 V, non-uniform and narrower weld appearance was formed. At the higher welding voltage, unstable welding processes with larger spatter induced discontinuous weld appearance. Only at the welding voltage of 12–14 V, uniform, continuous weld appearances were obtained. In a short, for Ti–Mg joint, optimized welding variables were followed: wire feed speed of 5.0 m/min, welding speed of 7.14 mm/s, and welding voltage of 12–14 V.

3.2. Microstructures and bonding mechanisms of Mg–Ti and Ti–Mg joints

Fig. 6 showed the cross sections of Mg–Ti and Ti–Mg joints. Fig. 7 presented the Mg–Ti phase diagram having a maximum solid solubility of 0.00043 at.% Ti in Mg in Ref. [27]. From Fig. 7, it indicated that neither solid solutions nor intermetallics form between Mg and Ti. Furthermore, the melting points of Mg and Ti are 649 °C and 1668 °C, respectively. This huge difference in melting points made it very difficult to melt both in a welding pool by traditional fusion welding. For Mg–Ti joint as shown in Fig. 1(a), during the joining process, while welding joint were occurred between the molten Mg AZ31B base metal and molten wire, brazing joint were developed between the molten weld metal and on the surface of local molten Ti. As a result, a welding–brazing joint was formed for Mg–Ti dissimilar metals. As shown in Fig. 6(a), a sound weld was composed of the weld metal, welding interface on the Mg AZ31B sheet and brazing interface between the weld metal and local molten Ti sheet. For Ti–Mg joint as shown in Fig. 6(b), when Ti sheet was displaced on the top of the Mg sheet, two brazing interfaces (A and B) between the weld metal and non-melted Ti sheet, and two welding interfaces between the weld metal and molten Mg sheet were formed, and thus the Ti–Mg joint was composed of weld metal, two brazing interfaces and two welding interfaces.

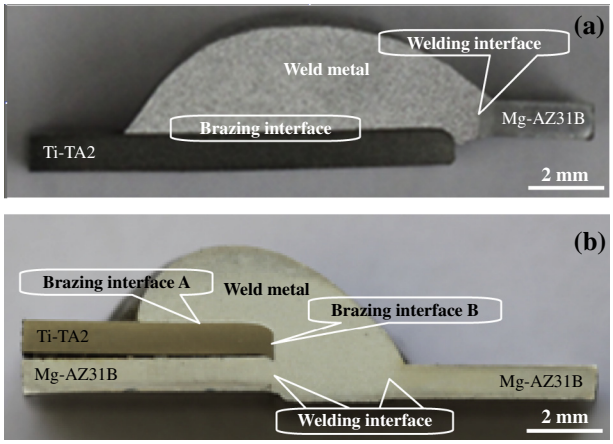

Fig. 6. Cross sections of two joints: (a) Mg–Ti joint (top Mg sheet–bottom Ti sheet), and (b) Ti–Mg joint (top Ti sheet–bottom Mg sheet).

Microstructures of the weld metal for two joints were almost the same and presented in Fig. 8. To understand the material properties of CMT welded Mg AZ31B to Ti TA2 with AZ61 wire, the microstructures of the weld metal were analyzed. Figs. 8–10 and Table 2 present the detailed microstructures and detailed EDS results of weld metal and welding interfaces, respectively. Since region 1 in Fig. 8(b) contains 93 at.% Mg and a small amount of O and Zn, the phase in region 1 is α-Mg solid solution. Region 2 in Fig. 8(b) contains 65.44 at.% O, 25.60 at.% Mg and a small amount of Al and Zn, and consequently the corresponding phase is likely an oxide inclusion. For the region 3, it contains 54.36 at.% Mg, 36.24 at.% Al, which is consistent with the β-$Al_{12}Mg_{17}$intermetallic. Based on these analyses, the microstructure of the weld metal is

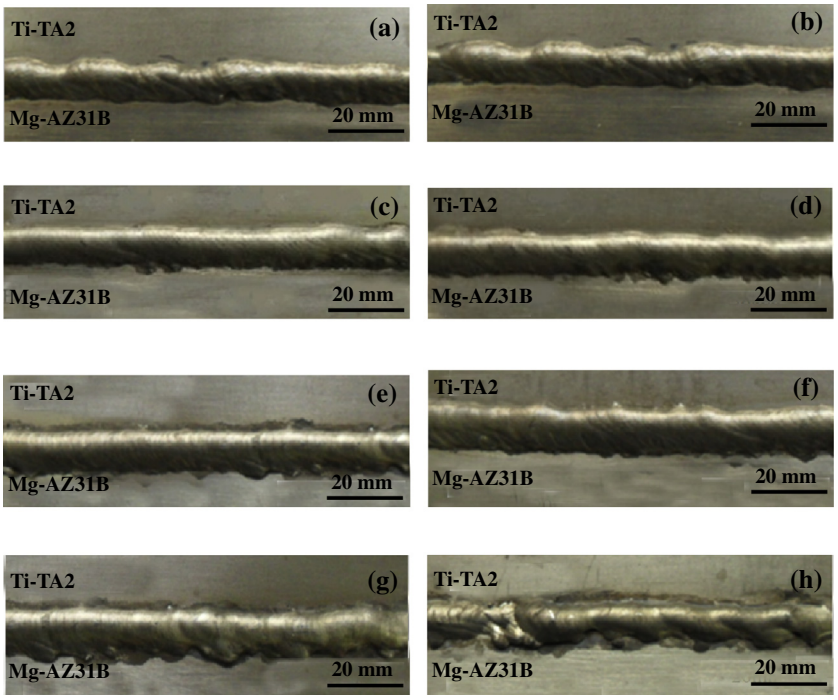

Fig. 5. Effects of welding voltage on weld appearance of Ti–Mg joint (top Ti sheet–bottom Mg sheet): (a) welding voltage of 10 V, (b) welding voltage of 11 V, (c) welding voltage of 12 V, (d) welding voltage of 13 V, (e) welding voltage of 14 V, (f) welding voltage of 15 V, (g) welding voltage of 17 V, and (h) welding voltage of 19 V.

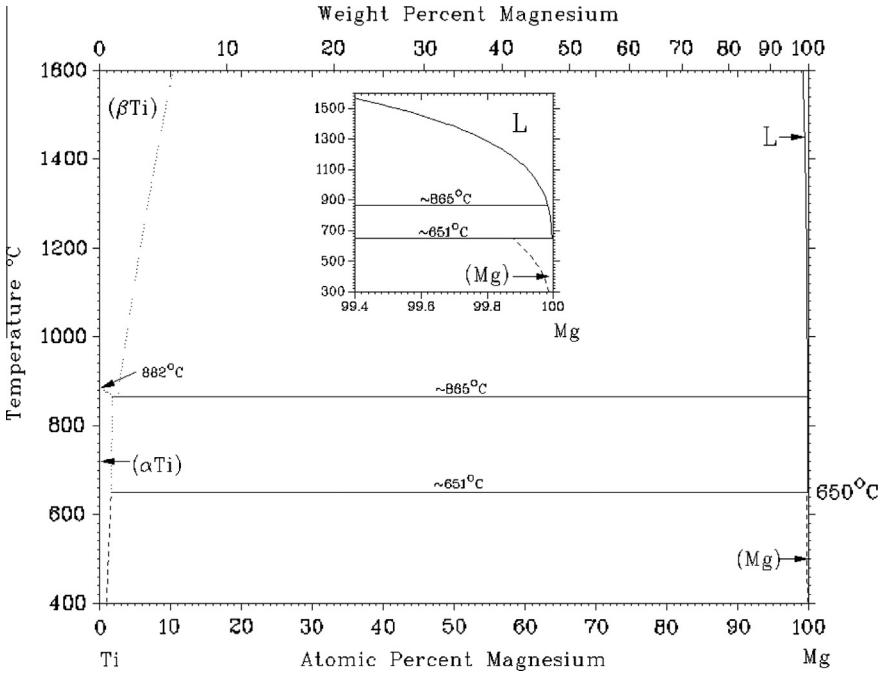

Fig. 7. The Mg–Ti binary alloy phase diagram.

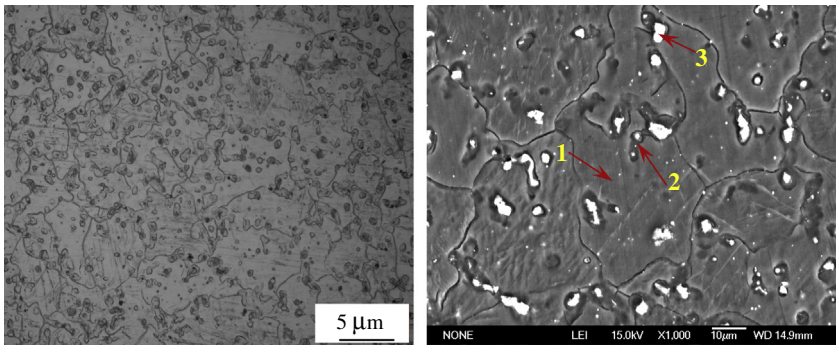

(a) (b)

Fig. 8. Microstructure of weld metal for Mg–Ti joint (top Mg sheet–bottom Ti sheet) and Ti–Mg joint (top Ti sheet–bottom Mg sheet): (a) weld metal by OM, and (b) weld metal by SEM.

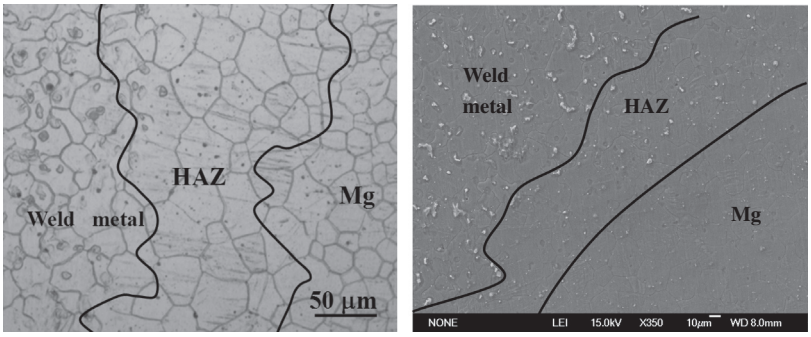

(a) (b)

Fig. 9. Microstructures of welding interface of the Mg–Ti joint (top Mg sheet–bottom Ti sheet): (a) microstructure of welding interface by OM, and (b) microstructure of welding interface by SEM.

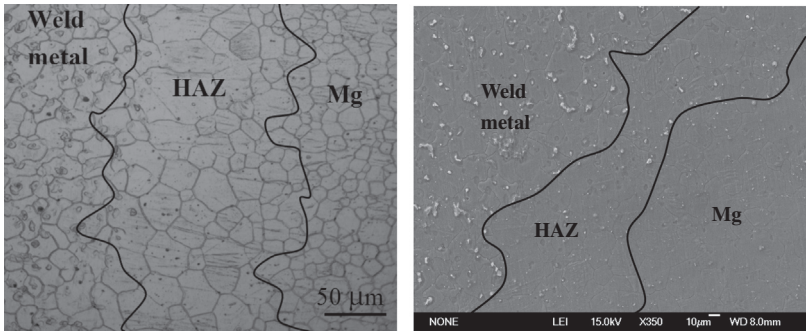

Fig. 10. Microstructures of welding interface of the Ti–Mg joint (top Ti sheet–bottom Mg sheet): (a) microstructure of welding interface by OM, and (b) microstructure of welding interface by SEM.

Table 2
EDS analysis results of various zones shown in Fig. 8(b).

Regions in Fig. 8(b)	Atomic content in percentage (at.%)				
	O	Fe	Mg	Al	Zn
1	4.24	–	93.00	–	4.44
2	65.44	–	25.60	5.65	1.28
3	2.90	–	54.36	36.24	6.50

composed of a α-Mg solid solution dendritic structure (denoted by region 1), which contains a few oxide inclusions (denoted by region 2), with the eutectic structure along the grain boundaries consisting of β-$Al_{12}Mg_{17}$ mesh intermetallic (denoted by region 3).

Figs. 9 and 10 presented the microstructures of welding interfaces for Mg–Ti joint and Ti–Mg joint respectively. From Figs. 9 and 10, the microstructures of welding interfaces for the two joints were similar. The grain of Mg heat affected zone (HAZ) became coarser at the effects of welding arc heat, which induced Mg HAZ softening.

Compared by the phase diagrams of Mg-steel and Mg–Ti, it was found that the joining of steel to magnesium alloy seems to have the same challenge as joining of titanium to magnesium alloy. Series results [18–20] indicated that the strength of dissimilar Mg-steel joints was mainly determined by the brazing interface between the molten Mg weld metal and non-molten galvanized steel sheets. To understand the bond mechanism at the brazing interface of the Mg–Ti joint, EDS line scanning results were also employed to analyze the brazing interface of the welded Mg AZ31B–Ti TA2 joints.

The microstructures of brazing interfaces for Mg–Ti joint and Ti–Mg joint are also similar. Fig. 11 indicates line scanning results of brazing interface for Mg/Ti and Ti/Mg CMT welding–brazing joints. As shown in Fig. 11, the gray image on the left-hand side is the pure Ti TA2, the image on the right-hand side is the weld metal, and the bright zone between the Ti TA2 sheet and weld metal is the brazing interface. EDS line analysis results (see Fig. 11) indicated that the narrow brazing interface zone was composed of Al, Ti, Mg and small Zn elements. In the brazing interface, higher Zn and higher Al contents can be found, and elements Ti and Mg only shows transition changed trends. EDS point analysis results of various zones in Fig. 11 were shown in Table 3. From Table 3, the weld metal near brazing interface is composed of α-Mg solid solution (denoted by arrow 5 in Fig. 11(a) and 9 in Fig. 11(b)) and $Mg_{17}Al_{12}$ intermetallic (denoted by arrow 4 in Fig. 11(a) and 10 in Fig. 11(b)). Moreover, the brazing interface layers are composed of the $Mg_{17}Al_{12}$ and Ti_3Al intermetallic compounds (Points 1, 2, 3 in Fig. 11(a)), $Mg_{17}Al_{12}$ (point 8 in Fig. 11(b)) and Ti_3Al intermetallic compound (point 7 in Fig. 11(b)).

To further identify the bonding mechanisms, XRD analysis of brazing interfaces were done as shown in Fig. 12. Results indicated that the brazing interfaces of Mg–Ti joint and Ti–Mg joint are almost the same, and are composed of Ti_3Al, $Mg_{17}Al_{12}$ and small $Mg_{0.97}Zn_{0.03}$ phases. Though the XRD peaks for Ti_3Al are shared peaks, it is still confirmed that Ti_3Al was formed in the brazing interface. It is because that XRD analysis was done on the fracture surface along brazing interface, the main peak is usually the peak of the base metal. If the peak of the base metal is deducted, Ti_3Al and $Mg_{17}Al_{12}$ are still the main compounds in the brazing interface. Moreover, a microhardness distribution across the interface has been done in Fig. 13. It indicates that transition brazing interface with higher hardness was also formed between Mg weld metal and Ti base metal, which is consistent with the results in Ref. [22]. It is because that element Al in the molten Mg AZ61 alloy aggregates to the liquid/solid interface, and interacts with Ti base metal at interface, finally Ti_3Al intermetallic is formed. It is not strange, such a interfacial structure is in accord with the thermodynamic characteristic of Al–Mg–Ti system. As we know, some elements in the wetting of molten alloy on solid surface are always tend to segregate at the surface of liquid or the liquid/solid interface, and the latter situation can be characterized by the adsorption energy, which indicate whether the solute element at infinite dilution in a liquid matrix segregate at liquid/solid interface or not, the adsorption energy can be written as following in Ref. [29]:

$$E^{\infty,SL}_{Al(Mg)} = m_1\left(\lambda_{TiAl} - \lambda_{MgAl} - \lambda_{TiMg}\right) \quad (1)$$

where $E^{\infty,SL}_{Al(Mg)}$ is the adsorption energy, the more negative the value of $E^{\infty,SL}_{Al(Mg)}$ indicates the stronger adsorption ability, m_1 is the structural parameter for the given system which has a positive value, λ_{ij} is the mole exchange energy for i and j. Further, λ_{TiAl} and λ_{TiMg} are −161.979 kJ/mol and 54.643 kJ/mol [30,31], λ_{MgAl} is range from −4.739 kJ/mol to −2.536 kJ/mol when temperature rises from the melting point to 1670 °C (the highest temperature we estimated may be the melting point of Ti) [32]. The value of $E^{\infty,SL}_{Al(Mg)}/m_1$ can be calculated easily in the range of −211.883–214.086 kJ/mol. Such a large negative value of $E^{\infty,SL}_{Al(Mg)}/m_1$ suggests that the molten Al–Mg alloy/Ti system should have Al segregation at liquid/solid interface. Further, the intermetallic Ti_3Al was formed by dissolution–precipitation reaction mechanism or precipitation in the cooling process. Moreover, some $Mg_{17}Al_{12}$ and $Mg_{0.97}Zn_{0.03}$ phases also be produced at the brazing interface. Therefore, elements Al and Zn in the AZ61 wire and AZ31B Mg base metal have a crucial effect on Mg–Ti joining.

3.3. Mechanical properties of Mg–Ti and Ti–Mg joints

The static tensile tests were carried out and the results were presented in Figs. 14–17.

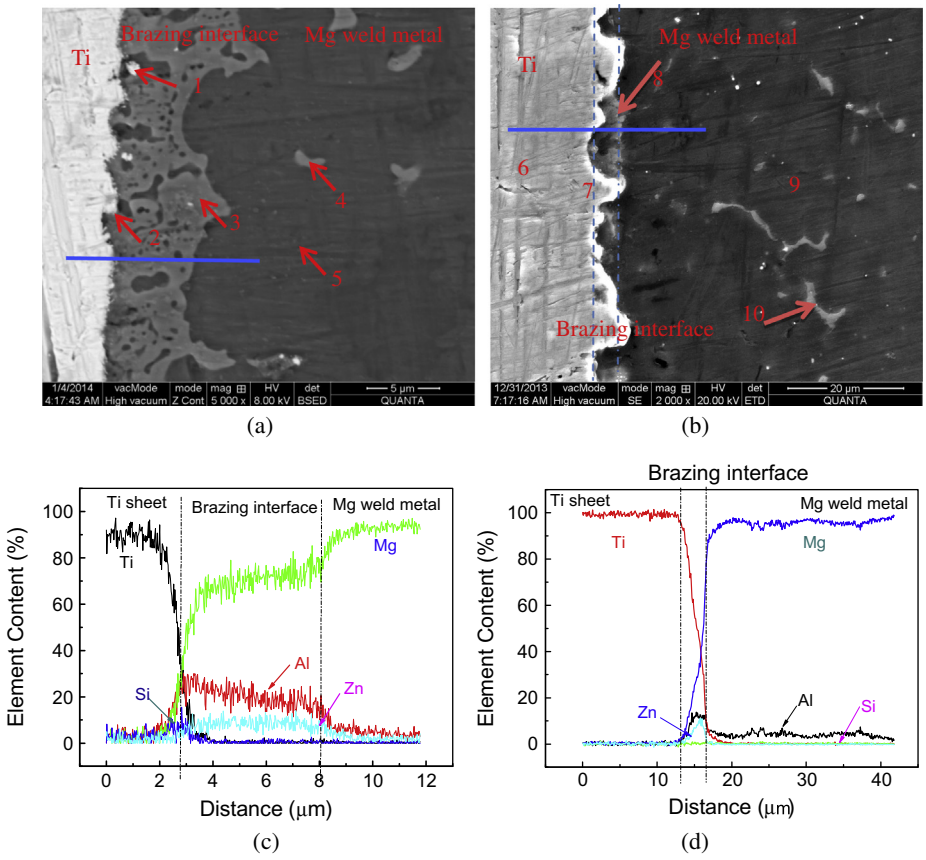

Fig. 11. Line scanning results of brazing interface for Mg–Ti joint (top Mg sheet–bottom Ti sheet) (a and c) and Ti–Mg joint (top Ti sheet–bottom Mg sheet) (b and d). (a) Magnified brazing interface in Fig. 6(a). (b) Magnified brazing interface B in Fig. 6(b). (c) Line scanning result along blue line in Fig. 11(a), and (d) line scanning result along blue line in Fig. 11(b). (For interpretation of the references to colour in this figure legend, the reader is referred to the web version of this article.)

Table 3
EDS point analysis results of various zones shown in Fig. 11.

Regions in Fig. 11	Atomic content in percentage (at.%)					Possible phases
	Mg	Al	Ti	Zn	Si	
1	51.1	30.4	12.4	2.5	1.4	$Mg_{17}Al_{12}$, Ti_3Al
2	52.2	17.2	21.2	7.5	2.0	$Mg_{17}Al_{12}$, Ti_3Al
3	63.5	28.3	4.0	3.6	0.7	$Mg_{17}Al_{12}$, Ti_3Al
4	74.4	23.3	0	2.3	0	$Mg_{17}Al_{12}$
5	94.4	5.0	0	0.5	0.2	α-Mg solid solution
6	1.0	0	98.5	0.2	0.3	Ti solid solution
7	12	9.2	73.3	0.2	5.2	Ti_3Al
8	74.8	21.3	1.6	2.1	0.2	$Mg_{17}Al_{12}$
9	97.5	2.3	0	0.2	0	α-Mg solid solution
10	77.9	19.5	0	2.6	0	$Mg_{17}Al_{12}$

Effects of wire feed speed on the mechanical properties of Mg–Ti joint was shown in Fig. 14. From Fig. 14, the effects of wire feed speed on tensile load were consistent with that of weld appearance. With increasing of the wire feed speed, tensile load firstly increased, and then decreased. At the lower wire feed speed range of 3.5–4.5 m/min, lower tensile load was obtained. It is attributed that lower heat input induces molten Ti base metal little, which further makes $Mg_{17}Al_{12}$, $Mg_{0.97}Zn_{0.03}$ and Ti_3Al produced in the brazing interface become smaller. Moreover, from Fig. 3, the discontinuous and undercutting weld appearance in the lower wire feed speed also led to lower tensile load. Only when wire feed speed of 5.0 m/min, welding speed of 7.14 mm/s and welding voltage of 10 V were used, the higher tensile load of 1.58 kN was reached. It is because the satisfied weld appearance and brazing interface were formed.

Effects of welding voltage on the mechanical properties of Mg–Ti joint were shown in Fig. 15. With increasing the welding voltage, tensile load firstly increased, and then decreased. When the welding voltage of 13 V was chosen, the best tensile load was obtained. At the lower welding voltage (lower heat input), little molten Ti sheet made the bonding of the joint become weaker. At the higher welding voltage, higher heat input induced the welding process become unstable with larger spatter and local undercutting, thus lower tensile load was reached. Only when suitable welding voltage of 13 V was set, the higher tensile load was obtained.

For Ti–Mg joint, the effects of welding voltage on tensile load were shown in Fig. 16. Similar phenomena and joining mechanisms can be found. When the welding voltage of 13.5 V was set, the optimized tensile load of 1.83 kN was obtained.

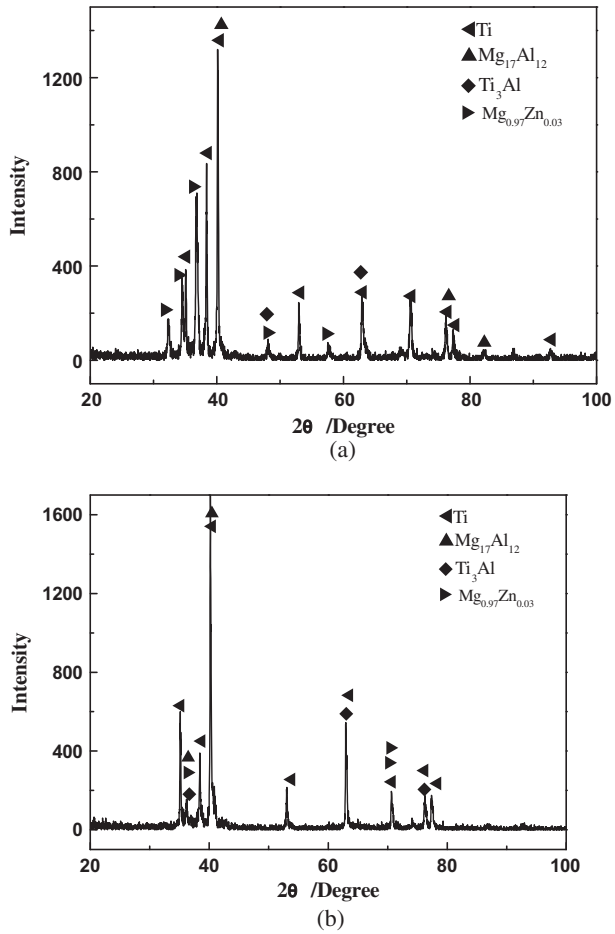

Fig. 12. XRD analysis of brazing interface: (a) Mg–Ti joint (top Mg sheet–bottom Ti sheet), and (b) Ti–Mg joint (top Ti sheet–bottom Mg sheet).

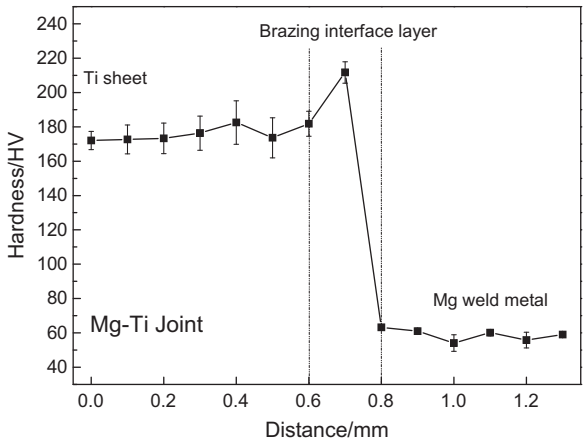

Fig. 13. Hardness distribution of brazing interface for Mg–Ti joint (top Mg sheet–bottom Ti sheet) joint.

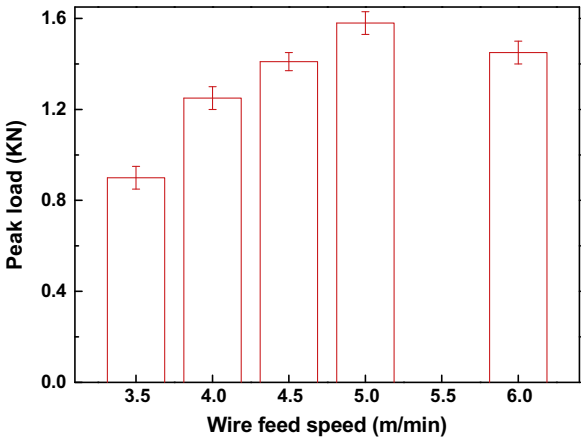

Fig. 14. Relationship between tensile load and wire feed speed for Mg–Ti joint (top Mg sheet–bottom Ti sheet).

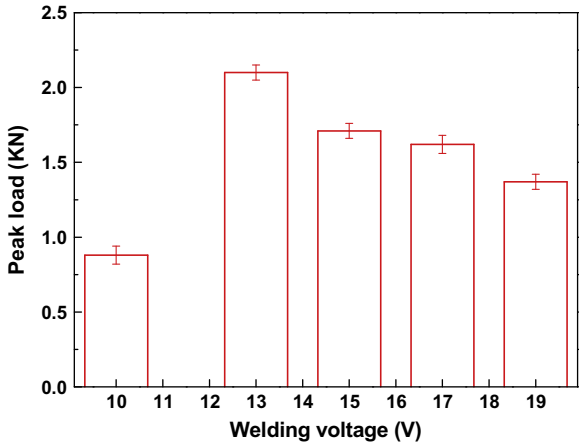

Fig. 15. Relationships between tensile load and welding voltage for Mg–Ti joint (top Mg sheet–bottom Ti sheet).

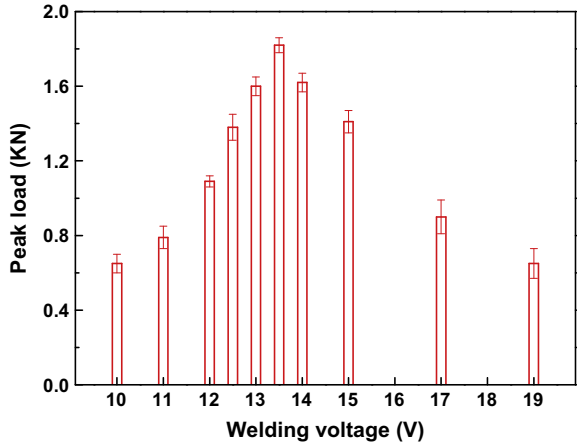

Fig. 16. Relationship between tensile load and welding voltage for Ti–Mg joint (top Ti sheet–bottom Mg sheet).

For two various lap-shear joints, though the cross sections of the joints were various as shown in Fig. 6, the bonding mechanisms of brazing interfaces were almost the same as shown in Figs. 8–12. Finally, the change trends of the tensile load were presented in Fig. 17. From Fig. 17, in the general, the tensile load of the Mg–Ti joint was higher than that of Ti–Mg joint. For Mg–Ti joint and Ti–Mg joint, to improve the tensile load of the joints, the local melting of Ti base metal was the key. However, the melting point of Mg wire was only 649 °C, the arc temperature made Ti sheet melt little. To overcome the dilemma, the Mg wire should deviate to Ti sheet. Gao et al. has indicated that the deviating distance was highly sensitive to weld appearance and tensile load [22]. About this issue, detailed study will be further concentrated in the future.

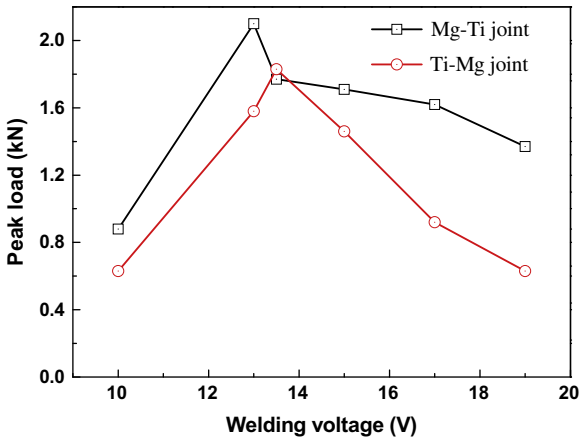

Fig. 17. Comparison of tensile load for Mg–Ti joint (top Mg sheet–bottom Ti sheet) and Ti–Mg joint (top Ti sheet–bottom Mg sheet).

4. Conclusions

Base on series studies of the effects of welding variables on weld appearance and tensile load for two joints, and analysis of microstructures and bonding mechanisms of the two joints, the followed conclusions can be obtained:

(1) Satisfied Mg–Ti joint and Ti–Mg joint can be performed at suitable welding variables with Mg AZ61 wire by CMT welding–brazing method.
(2) For Mg–Ti joint, when welding voltage of 13 V, wire feed speed of 5.0 m/min and welding speed of 7.14 mm/s were chosen, satisfied weld appearance and higher tensile load of 2.10 kN can be obtained. For Ti–Mg joint, when welding voltage of 13.5 V, wire feed speed of 5.0 m/min and welding speed of 7.14 mm/s were chosen, satisfied weld appearance and higher tensile load of 1.83 kN can be obtained.
(3) Typical brazing–welding joints can be formed. A sound Mg–Ti joint was composed of the weld metal, fusion zone on the Mg AZ31 sheet and the brazing interface between the weld metal. However, a sound Ti–Mg joint was composed of weld metal, two brazing interface and two welding interfaces.
(4) The brazing interface is mainly composed of Ti_3Al, $Mg_{17}Al_{12}$ and $Mg_{0.97}Zn_{0.03}$ intermetallics. Elements Al and Zn in the Mg base metal and Mg wire are crucial to join successfully Mg and Ti base metals.

Acknowledgements

This work was financially supported by National Nature Science Foundation of China (No. 51265028). The authors wish to thank the editors and reviewers for their comments and suggestions.

References

[1] A.N. Alhazaa, T.I. Khan, J. Alloys Comp. 494 (2010) 351–358.
[2] Z.P. Ma, Mater. Des. 45 (2013) 72–79.
[3] X.G. Chen, J.C. Yan, S.C. Ren, J.H. Ren, J.H. Wei, Q. Wang, Mater. Lett. 95 (2013) 197–200.
[4] R. Cao, J.H. Sun, J.H. Chen, Sci. Technol. Weld. Join. 18 (2013) 425–433.
[5] T. Saeid, A. Abdollah-zadeh, B. Sazgari, J. Alloys Comp. 490 (2010) 652–655.
[6] S.J. Lee, H. Nakamura, Y. Kawahito, S. Katayama, Sci. Technol. Weld. Join. 1 (19) (2014) 111–118.
[7] D. Zuo, S.S. Hu, J.Q. Shen, Z.Q. Xue, Mater. Des. 58 (2014) 357–362.
[8] J.L. Song, S.B. Lin, C.L. Yang, C.L. Fan, J. Alloys Comp. 488 (2009) 217–222.
[9] C. Dharmendra, K.P. Rao, J. Wilden, S. Reich, Mater. Sci. Eng. A 528 (2011) 1497–1503.
[10] R. Cao, Q. Huang, J.H. Chen, Pei-Chung Wang, J. Alloys Comp. 585 (2014) 622–632.
[11] R. Cao, G. Yu, J.H. Chen, J. Mater. Process. Technol. 213 (2013) 1753–1763.
[12] H.T. Zhang, J.C. Feng, P. He, B.B. Zhang, Mater. Sci. Eng. A 499 (2009) 111–113.
[13] Y.L. Zhou, Q. Lin, J. Alloys Comp. 589 (2014) 307–313.
[14] R. Cao, Z. Feng, J.H. Chen, Mater. Des. 53 (2014) 192–201.
[15] R.K. Shiue, S.K. Wu, C.H. Chan, J. Alloys Comp. 372 (2004) 148–157.
[16] R. Cao, Z. Feng, J.H. Chen, Mater. Des. 532 (2014) 192–201.
[17] R. Cao, J.Y. Yu, J.H. Chen, Weld. J. 92 (2013) 274s–282s.
[18] L.M. Liu, X.D. Qi, Mater. Des. 31 (2010) 3960–3963.
[19] X.D. Qi, G. Song, Mater. Des. 31 (2010) 605–609.
[20] T. Pan, Z. Feng, M. Santella, J. Chen, SAE Int. J. Mater. Man. 6 (2) (2013) 271–278.
[21] T. DebRoy, H.K.D.H. Bhadeshia, Sci. Technol. Weld. Join. 4 (2010) 266–270.
[22] M. Gao, Z.M. Wang, X.Y. Li, X.Y. Zeng, Metall. Mater. Trans. A 43 (2012) 163–172.
[23] M. Gao, Z.M. Wang, J. Yan, X.Y. Zeng, Sci. Technol. Weld. Join. 16 (2011) 488–496.
[24] J.T. Xiong, F.S. Zhang, J.L. Li, W.D. Huang, Rare Met. Mater. Eng. 35 (2006) 1677.
[25] Li Rui-di, Li Jing-long, Xiong Jiang-tao, Zhang Fu-sheng, Zhao Ke, Ji Cheng-zhong, Trans. Nonferrous Met. Soc. China 22 (2012) 2665–2671.
[26] M. Aonuma, K. Nakata, Mater. Sci. Eng. B 177 (2012) 543–548.
[27] C.M. Liu, X.R. Zhu, H.T. Zhou. Hunan: Central South University Press, 2006.
[28] X.R. Yang, Arch Weld. Machine 36 (2006) 5–7.
[29] N. Eustathopoulos, M.G. Nicholas, B. Drevet, Wettability at High Temperatures[M], Elsevier, 1999.
[30] A.R. Miedema, A.K. Niessen, F.R. de Boer, R. Boom, W.C.M. Matten, Cohesion in Metals: Transition Metal Alloys [J], North-Holland, Amsterdam, 1989.
[31] R.F. Zhang, S.H. Sheng, B.X. Liu, Chem. Phys. Lett. 442 (2007) 511–514.
[32] Y. Tang, Y. Du, L.J. Zhang, X.M. Yuan, George Kaptay, Thermochim. Acta 527 (2012) 131–142.